ACCURATE PREDICTION OF SPRING-BACK PHENOMENON BY SUBLOADING SURFACE MODEL

MOTOHARU TATEISHI AND KOICHI HASHIGUCHI

MSC Software Ltd. (MSC)
Shinjuku First West 8F
23-7, Nishishinjuku, 1-chome,
Shinjuku-ku, Tokyo 160-0023, Japan
e-mail: motoharu.tateishi@mscsoftware.com, web page: http://www.mscsoftware.com
e-mail: koichi.hashiguchi@mscsoftware.com, web page: http://www.mscsoftware.com

Key words: Elastoplastic deformation, Finite element analysis, Spring back, Subloading surface model.

Abstract. The subloading surface model possesses the distinguished capability to describe the plastic strain rate for the rate of stress inside the yield surface accurately and the stress-controlling function to pull-back the stress to the yield surface even when it goes out from the yield surface in the numerical calculation. The spring-back phenomenon of the high strength steel is analyzed by the commercial software Marc implemented the subloading surface model and thus the high accuracy of the simulation is verified in this article.

1 INTRODUCTION

The subloading surface (Hashiguchi) model [1] [2] [3] [4] possesses the distinguished advantages which are not furnished in the other elastoplasticity models, i.e. the conventional elastoplasticity model and the unconventional models (cyclic elastoplasticity models), e.g. the multi surface model [5], the two surface model [6] and the superposed-kinematic hardening model [7] inheriting the yield surface enclosing purely-elastic domain from the conventional elastoplasticity model. In particular, the smooth elastic-plastic transition is always described by excluding a purely-elastic domain and the automatic controlling function to attract the stress to the yield surface is furnished in the subloading surface model. Consequently, it provides the high ability in both aspects of the accuracy for the description of physical property and the efficiency of numerical calculation. The subloading surface model has been implemented in the commercial software Marc in MSC Software Corporation [8] as the standard installation by the name “Hashiguchi model”, which can be used by all Marc users (contractors). Nowadays, the high tensile (strength) steel sheets and aluminum sheets exhibiting far larger springback than the ordinary mild steel sheets are widely used in automobile industries, etc. The springback cannot be described by the constitutive models which use the yield surface enclosing a purely-elastic domain, i.e. the conventional model and the cyclic kinematic hardening models (multi-surface, two-surface and superposed kinematic hardening models), since a plastic strain rate in the unloading process is not described appropriately by these models. The spring-back phenomenon of the high strength steel is analyzed by the Marc so that the high accuracy of the

simulation is verified in this article, illustrating several numerical results including the comparison with experimental result.

2 ADDITIVE DECOMPOSITION OF STRAIN INCREMENT AND ELATIC STRAIN INCREMENT

The infinitesimal strain tensor $\boldsymbol{\varepsilon}$ is additively decomposed into the elastic strain tensor $\boldsymbol{\varepsilon}^e$ and the plastic strain tensor $\boldsymbol{\varepsilon}^p$ as follows:

$$\boldsymbol{\varepsilon}=\boldsymbol{\varepsilon}^e+\boldsymbol{\varepsilon}^p,\quad d\boldsymbol{\varepsilon}=d\boldsymbol{\varepsilon}^e+d\boldsymbol{\varepsilon}^p \tag{1}$$

First, the elastic strain $\boldsymbol{\varepsilon}^e$ and its increment are linearly related to the Cauchy stress tensor $\boldsymbol{\sigma}$ and its increment as follows:

$$\boldsymbol{\varepsilon}^e=\mathbf{E}^{-1}:\boldsymbol{\sigma},\quad d\boldsymbol{\varepsilon}^e=\mathbf{E}^{-1}:d\boldsymbol{\sigma} \tag{2}$$

where the fourth-order tensor $\mathbf{E}$ is the elastic modulus tensor which is given by

$$E_{ijkl}=\frac{\nu E}{(1+\nu)(1-2\nu)}\delta_{ij}\delta_{kl}+\frac{E}{2(1+\nu)}(\delta_{ik}\delta_{jl}+\delta_{il}\delta_{jk}) \tag{3}$$

E and ν are the Yong's modulus and the Poisson's ratio, respectively.

3. SUBLOADING SURFACE MODEL

The concept and the constitutive equation of the subloading surface model [1][4] is described concisely in this section.

3.1 Yield surface and its evolution

First, we incorporate the following Mises yield condition with the isotropic and the kinematic hardenings is adopted.

$$f(\hat{\boldsymbol{\sigma}})=F(H) \tag{4}$$

with

$$f(\hat{\boldsymbol{\sigma}})=\sigma^{eq}=\sqrt{3/2}\,\|\hat{\boldsymbol{\sigma}}'\| \tag{5}$$

$$\hat{\boldsymbol{\sigma}}\equiv\boldsymbol{\sigma}-\boldsymbol{\alpha} \tag{6}$$

where $F(H)$ is the isotropic hardening function of the isotropic hardening variable H and $\boldsymbol{\alpha}\,(=\boldsymbol{\alpha}')$ is the kinematic hardening variable and their evolution rules are given as follows:

$$F(H)=F_0\{1+h_1[1-\exp(-h_2H)]\},\quad F'=dF/dH=F_0\,h_1\,h_2\exp(-h_2H) \tag{7}$$

$$H=\varepsilon^{eqp},\quad dH=d\varepsilon^{eqp}=\sqrt{2/3}\,\|d\boldsymbol{\varepsilon}^{p\prime}\| \tag{8}$$

$$d\boldsymbol{\alpha}=c_k\left(d\boldsymbol{\varepsilon}^p-\frac{1}{\sqrt{3/2}\zeta F}\|d\boldsymbol{\varepsilon}^p\|\boldsymbol{\alpha}\right) \tag{9}$$

where σ^{eq} is the equivalent stress and ε^{eqp} is the equivalent plastic strain. h_1, h_2, c_k and ζ are the material constants.

3.2 Subloading surface

The subloading surface model is premised on the following basic concept in order to describe the plastic strain increment induced by the rate of stress inside the yield surface, renames the *normal-yield surface.*

Subloading surface concept: *The stress approaches the yield surface when the plastic strain increment is induced, exhibiting a continuous variation of tangent modulus, but it recedes from the yield surface when only the elastic strain increment is induced*.

Then, the *subloading surface* which passes through the current stress point and is similar to the yield surface, renamed the *normal-yield surface*, is introduced and the ratio of the size of the subloading surface to that of the normal-yield surface is adopted as the measure designating the degree of approaching to the normal-yield surface.

The subloading surface is given as follows (see Fig. 1).

$$f(\bar{\boldsymbol{\sigma}}) = RF(H) \tag{10}$$

where

$$\bar{\boldsymbol{\sigma}} \equiv \boldsymbol{\sigma} - \bar{\boldsymbol{\alpha}} \tag{11}$$

$\bar{\boldsymbol{\alpha}}$ stands for the conjugate (similar) point in the subloading surface to the point $\boldsymbol{\alpha}$ in the normal-yield surface. The function $f(\bar{\boldsymbol{\sigma}})$ is given explicitly conforming to Eq. (5) as follows:

$$f(\bar{\boldsymbol{\sigma}}) = \sqrt{3/2}\,\|\bar{\boldsymbol{\sigma}}'\| \tag{12}$$

By letting $\mathbf{c}$ denote the center of similarity of the normal-yield and the subloading surfaces, i.e. the similarity-center, which is called *elastic-core* since the most elastic deformation behavior is induced when the stress lies on it fulfilling $R = 0$ as will be explained later, the following relation holds (see Figure 1).

$$\mathbf{c} - \bar{\boldsymbol{\alpha}} = R(\mathbf{c} - \boldsymbol{\alpha}) \tag{13}$$

which yields

$$\bar{\boldsymbol{\alpha}} = \mathbf{c} - R\,\hat{\mathbf{c}} \tag{14}$$

$$\bar{\boldsymbol{\sigma}} = \tilde{\boldsymbol{\sigma}} + R\,\hat{\mathbf{c}} \tag{15}$$

where

$$\begin{cases} \hat{\mathbf{c}} \equiv \mathbf{c} - \boldsymbol{\alpha} \\ \tilde{\boldsymbol{\sigma}} \equiv \boldsymbol{\sigma} - \mathbf{c} \end{cases} \tag{16}$$

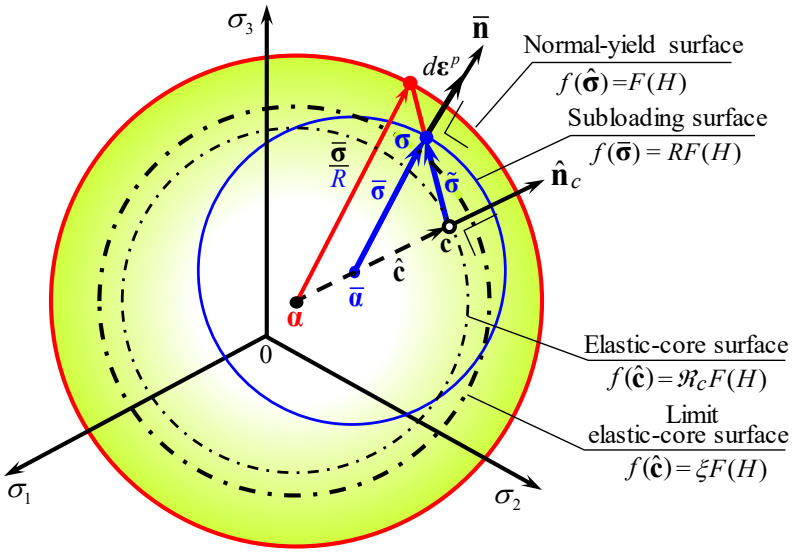

Fig. 1. Normal-yield, subloading and elastic-core surfaces.

The evolution rule of the normal-yield ratio is given by

$$dR = U(R)\| d\boldsymbol{\varepsilon}^p \| \quad \text{for } d\boldsymbol{\varepsilon}^p \neq \mathbf{O} \tag{17}$$

where

$$U(R) = u\cot\left(\frac{\pi}{2}\frac{\langle R-R_e\rangle}{1-R_e}\right) \tag{18}$$

The evolution rule of the kinematic hardening rule is given by

$$d\boldsymbol{\alpha} = c_k\left(d\boldsymbol{\varepsilon}^p - \frac{1}{\sqrt{3/2}\zeta F}\| d\boldsymbol{\varepsilon}^p \|\boldsymbol{\alpha}\right) \tag{19}$$

Now, let the following *elastic-core surface* (see Fig. 1) be introduced, which always passes through the elastic-core $\mathbf{c}$ and maintains a similarity to the normal-yield surface with respect to the kinematic-hardening variable $\boldsymbol{\alpha}$.

$$f(\hat{\mathbf{c}}) = \mathcal{R}_c F(H), \text{ i.e. } \mathcal{R}_c = f(\hat{\mathbf{c}})/F(H) \tag{20}$$

where $\mathcal{R}_c$ designates the ratio of the size of the elastic-core surface to that of the normal-yield surface and thus let it be called the *elastic-core yield ratio*. The function $f(\hat{\mathbf{c}})$ is given for Eq. (5) by

$$f(\hat{\mathbf{c}}) = \sqrt{3/2}\,\|\hat{\mathbf{c}}\| \tag{21}$$

The translation rule of elastic-core is given by

$$d\mathbf{c} = c\left(d\boldsymbol{\varepsilon}^p - \frac{\mathcal{R}_c}{\xi}\| d\boldsymbol{\varepsilon}^p \|\hat{\mathbf{n}}_c\right) \tag{22}$$

where ξ (<1) is material constant, c is a material parameter and

$$\hat{\mathbf{n}}_c \equiv \frac{\partial f(\hat{\mathbf{c}})}{\partial \mathbf{c}} \Big/ \Big\| \frac{\partial f(\hat{\mathbf{c}})}{\partial \mathbf{c}} \Big\| = \frac{\hat{\mathbf{c}}}{\|\hat{\mathbf{c}}\|} \quad (\|\hat{\mathbf{n}}_c\|=1) \tag{23}$$

In order to describe the Masing effect [10], the material parameter u involved in Eq. (18) for the function $U(R)$ is extended as follows:

$$u = \bar{u} \exp(u_c \mathfrak{R}_c C_\sigma) \quad (\bar{u} \exp(-u_c \xi) \le u \le \bar{u} \exp(u_c \xi)) \tag{24}$$

where $\bar{u}$ (average value of u), u_c are the material constants and

$$C_\sigma \equiv \hat{\mathbf{n}}_c : \bar{\mathbf{n}} \quad (-1 \le C_\sigma \le 1) \tag{25}$$

The increment form of Eq. (14) leads to

$$d\bar{\boldsymbol{\alpha}} = R d\boldsymbol{\alpha} + (1-R) d\mathbf{c} - dR\hat{\mathbf{c}} \tag{26}$$

Substituting Eqs. (17), (19) and (22) into Eq. (26), one obtains

$$d\bar{\boldsymbol{\alpha}} = c_k R\Big(d\boldsymbol{\varepsilon}^p - \frac{1}{b_k}\|d\boldsymbol{\varepsilon}^p\|\boldsymbol{\alpha}\Big) + c(1-R)\Big(d\boldsymbol{\varepsilon}^p - \frac{\mathcal{R}_c}{\chi}\|d\boldsymbol{\varepsilon}^p\|\hat{\mathbf{n}}_c\Big) - U(R)\hat{\mathbf{c}}\|d\boldsymbol{\varepsilon}^p\| \tag{27}$$

The increment of Eq. (10) leads to the consistency condition of the subloading surface:

$$\frac{\partial f(\bar{\boldsymbol{\sigma}})}{\partial \bar{\boldsymbol{\sigma}}} : d\boldsymbol{\sigma} - \frac{\partial f(\bar{\boldsymbol{\sigma}})}{\partial \bar{\boldsymbol{\sigma}}} : d\bar{\boldsymbol{\alpha}} - RdF - dRF = 0 \tag{28}$$

3.3 Plastic strain increment

Adopt the associated flow rule for the subloading surface:

$$d\boldsymbol{\varepsilon}^p = \bar{\mathbf{n}} d\bar{\lambda} \quad (d\bar{\lambda} = \|d\boldsymbol{\varepsilon}^p\| > 0) \tag{29}$$

where $d\bar{\lambda}$ is the plastic multiplier and

$$\bar{\mathbf{n}} \equiv \frac{\partial f(\bar{\boldsymbol{\sigma}})}{\partial \bar{\boldsymbol{\sigma}}} \Big/ \Big\| \frac{\partial f(\bar{\boldsymbol{\sigma}})}{\partial \bar{\boldsymbol{\sigma}}} \Big\| = \frac{\bar{\boldsymbol{\sigma}}'}{\|\bar{\boldsymbol{\sigma}}'\|} = \bar{\mathbf{n}}' \quad (\|\bar{\mathbf{n}}\|=1) \tag{30}$$

Substituting Eq. (29) into Eqs. (7), (17), (19) and (22), one has

$$dF = F' dH = F' f_H \|d\boldsymbol{\varepsilon}^p\| \tag{31}$$

$$dR = U(R) d\bar{\lambda} \tag{32}$$

$$d\boldsymbol{\alpha} = d\bar{\lambda} \bar{\mathbf{f}}_{kn} \tag{33}$$

$$d\mathbf{c} = d\bar{\lambda} \bar{\mathbf{f}}_{cn} \tag{34}$$

where

$$f_H = \sqrt{2/3} \tag{35}$$

$$\bar{\mathbf{f}}_{kn} \equiv c_k\Big(\bar{\mathbf{n}} - \frac{1}{\sqrt{3/2}\zeta F}\boldsymbol{\alpha}\Big) \tag{36}$$

$$\bar{\mathbf{f}}_{cn} \equiv c\Big(\bar{\mathbf{n}} - \frac{\mathcal{R}_c}{\xi}\|d\boldsymbol{\varepsilon}^p\|\hat{\mathbf{n}}_c\Big) \tag{37}$$

The substitutions of Eqs. (31), (32), (33) and (34) into Eq. (28) leads to

$$\bar{\mathbf{n}}:d\boldsymbol{\sigma}-\bar{\mathbf{n}}:\left[\sqrt{\frac{2}{3}}\frac{F'}{F}d\bar{\lambda}\bar{\boldsymbol{\sigma}}+R\bar{\mathbf{f}}_{kn}d\bar{\lambda}+(1-R)\bar{\mathbf{f}}_{cn}d\bar{\lambda}+\frac{U}{R}d\bar{\lambda}\tilde{\boldsymbol{\sigma}}\right]=0 \tag{38}$$

from which the plastic multiplier $d\bar{\lambda}$ and the plastic strain increment $d\boldsymbol{\varepsilon}^p$ are given as follows:

$$d\bar{\lambda}=\frac{\bar{\mathbf{n}}:d\boldsymbol{\sigma}}{\bar{M}^p},\quad d\boldsymbol{\varepsilon}^p=\frac{\bar{\mathbf{n}}:d\boldsymbol{\sigma}}{\bar{M}^p}\bar{\mathbf{n}} \tag{39}$$

where

$$\bar{M}^p=\bar{\mathbf{n}}:\left[\sqrt{\frac{2}{3}}\frac{F'}{F}\bar{\boldsymbol{\sigma}}+R\bar{\mathbf{f}}_{kn}+(1-R)\bar{\mathbf{f}}_{cn}+\frac{U}{R}\tilde{\boldsymbol{\sigma}}\right] \tag{40}$$

3.4 Stain increment vs. stress increment relations

The strain increment is given by substituting Eqs. (2) and (39) into Eq. (1) as follows:

$$d\boldsymbol{\varepsilon}=\mathbf{E}^{-1}:d\boldsymbol{\sigma}+\frac{\bar{\mathbf{n}}:d\boldsymbol{\sigma}}{\bar{M}^p}\bar{\mathbf{n}}=\left(\mathbf{E}^{-1}+\frac{\bar{\mathbf{n}}\otimes\bar{\mathbf{n}}}{\bar{M}^p}\right):d\boldsymbol{\sigma} \tag{41}$$

from which the plastic multiplier described in terms of the strain increment, denoted by $d\bar{\Lambda}$ instead of $d\bar{\lambda}$, in the flow rule of Eq. (29) is given as follows:

$$d\bar{\Lambda}=\frac{\bar{\mathbf{n}}:\mathbf{E}:d\boldsymbol{\varepsilon}}{\bar{M}^p+\bar{\mathbf{n}}:\mathbf{E}:\bar{\mathbf{n}}},\quad d\boldsymbol{\varepsilon}^p=\frac{\bar{\mathbf{n}}:\mathbf{E}:d\boldsymbol{\varepsilon}}{\bar{M}^p+\bar{\mathbf{n}}:\mathbf{E}:\bar{\mathbf{n}}}\bar{\mathbf{n}} \tag{42}$$

The stress increment is given from Eq. (41) with Eq. (42) as follows:

$$d\boldsymbol{\sigma}=\mathbf{E}:d\boldsymbol{\varepsilon}-\frac{\bar{\mathbf{n}}:\mathbf{E}:d\boldsymbol{\varepsilon}}{\bar{M}^p+\bar{\mathbf{n}}:\mathbf{E}:\bar{\mathbf{n}}}\mathbf{E}:\bar{\mathbf{n}}=\left(\mathbf{E}-\frac{\mathbf{E}:\bar{\mathbf{n}}\otimes\bar{\mathbf{n}}:\mathbf{E}}{\bar{M}^p+\bar{\mathbf{n}}:\mathbf{E}:\bar{\mathbf{n}}}\right):d\boldsymbol{\varepsilon} \tag{43}$$

The loading criterion is given as follows (Hashiguchi, 2000, 2017):

$$\begin{cases}d\boldsymbol{\varepsilon}^p\neq\mathbf{O} & \text{for } \bar{\mathbf{n}}:\mathbf{E}:d\boldsymbol{\varepsilon}>0\\ d\boldsymbol{\varepsilon}^p=\mathbf{O} & \text{for } \bar{\mathbf{n}}:\mathbf{E}:d\boldsymbol{\varepsilon}\le 0\end{cases} \tag{44}$$

4 IMPLEMENTATION OF SUBLOADING SURFACE MODEL TO IMPLICIT NONLINEAR FEA CODE

The subloading surface elastoplastic constitutive model innovated by Hashiguchi has rich functionalities describing plasticity phenomena such as isotropic hardening, kinematic hardening, marsing effect, stagnation, tangential plasticity and so on in addition to the most beneficial scheme of smooth transition description of elastic to elastoplastic region. In order to implement these full functionalities of subloading surface model, stress integration is performed explicitly so-called forward Euler integration method. With the conventional explicit integration scheme for nonlinear finite element analysis such as explicit creep analysis, program can not take large time step size due to stability limit. This is critical disadvantage of explicit integration method in general. Therefore, we tried to invent new solution scheme using explicit stress integration method for the implementation of subloading surface model into Marc general purpose finite element code mainly used statically loaded nonlinear analysis.

4.1 Forward Euler stress integration

The stress calculation phase occurs twice in nonlinear finite element software, internal force calculation before matrix solution phase for incremental displacement calculation and stress recovery phase after incremental displacement calculation. Total stress is calculated using incremental strain converted with incremental displacement in case of additive decomposition based large displacement finite element analysis. In case of large time step is taken for speed performance purpose, stress integration based on forward Euler fails due to excessive incremental strain, this characteristic called stability problem in explicit time step integration scheme. In order to resolve this stability limit problem, we developed a scheme that incremental strain is subdivide into small enough incremental strain then total incremental stress calculated using multiple sub-steps, hereafter called SSM Strain Subdivided Method. This logic requires multiple stress calculation steps within a single global stiffness matrix solution step that consumes lots of calculation time and also difficult to parallelize efficiently. In the other hand, element stiffness calculation and stress recovery phase can be easily parallelized by Domain Decomposition Method, hereafter called DDM, or OpenMP based multi-threading.

Fig. 2 illustrates the FEA model used for numerical experiment in order to investigate the required minimum subdivided strain increment for SSM. Model consists of single cubic element with 1mm edge length.

The material is elastic-plastic with material constants of Young's modulus, Poisson's ratio and initial yield stress used here are 170000 MPa, 0.3 and 510 MPa, respectively. The hardening coefficients, evolution of normal-yield ratio are defined as follows;

Isotropic hardening parameter:	h_1=0.61, h_2=170
Kinematic hardening parameter:	Ck=5200 MPa, ζ =0.2
Evolution of normal-yield ratio:	$\bar{u}$ =60, u_c=5, R_e=0.5

The face loads are applied on the top face of the mesh. The amplitude of the load is 830 MPa with pulsating cyclic history as shown in **Fig. 3**

The three different limit strain cases were tested, case1 with limit strain of 1.0d-3, case2 with limit strain of 1.0d-4 and case3 with limit strain of 1de-5. **Fig. 4** shows the numerical experiment result. From this numerical experiment result for limit strain impact to analysis stability and accuracy, limit strain of 1.0d-3 is too large and showed different result from other two cases and limit strain of 1.0d-4 and 1.0d-5 cases showed acceptable result. 1.0d-3 of strain is similar level of elastic limit of steel material and applying this level of strain in single stress calculation step is obviously causes accuracy problem. We selected limit strain of 1/20 of initial elastic strain obtained by Young's modulus and initial yield stress.

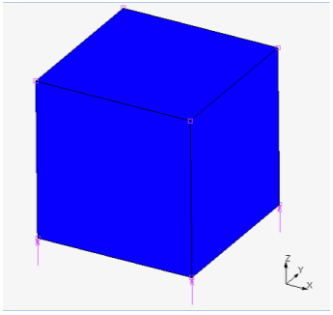

Fig. 2 Finite element model for SSM numerical experiment

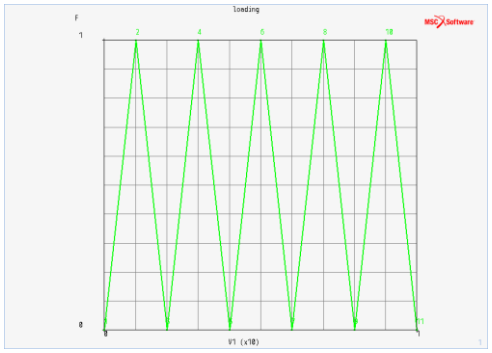

Fig. 3 Pulsating Cyclic Load History

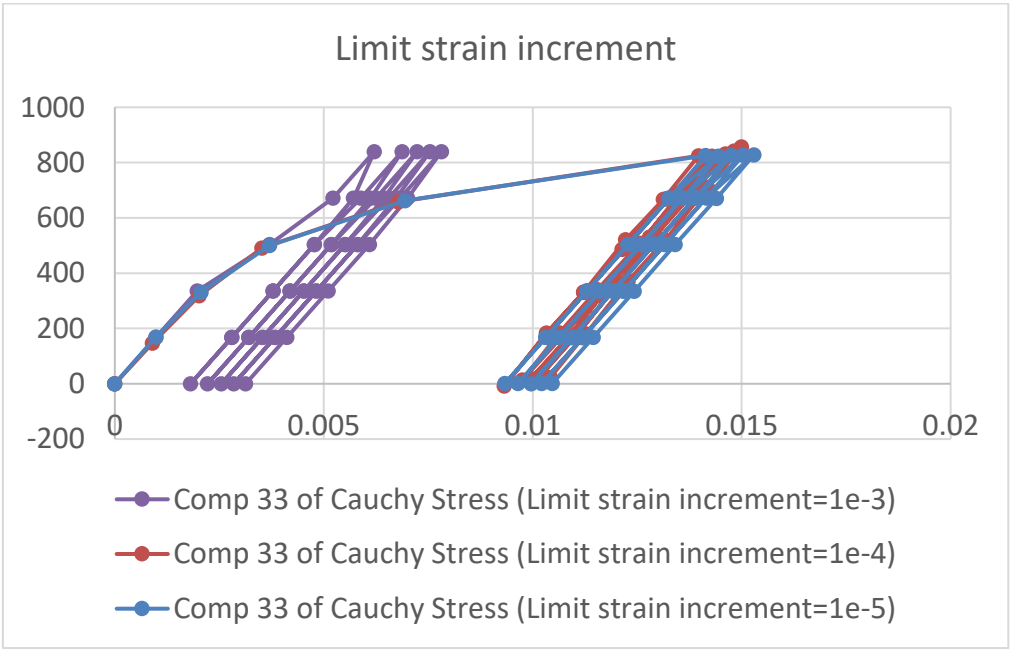

Fig. 4 Numerical experiment result with different limit strain

4.2 Mid-point tangential stiffness evaluation

With the SSM program work flow, tangential stiffness matrix is evaluated multiple times since incremental strain is subdivide and stress integration calculation occurs multiple times

within a Newton Raphson iteration. We conducted a series of numerical experiments to find the best tangential stiffness evaluation timing, beginning of the increment, mid-point of the increment or end of the increment using the same FEA model in the previous section and selected mid-point tangential stiffness evaluation scheme that gives accuracy and stability.

5 SPRINGBACK ANALYSES

The metal forming analyses are of importance in the industrial production. The analysis of the springback by use of the subloading surface model will be described in here.

The high strength steel sheets and aluminum sheets exhibiting far larger springback than ordinary mild steel sheets are widely used in automobile industries. The springback cannot be described by the constitutive models which use the yield surface enclosing a purely-elastic domain, i.e. the conventional model and the cyclic kinematic hardening models (multi-surface, two-surface and superposed kinematic hardening models), since a plastic strain rate in the unloading process is not described appropriately by these models. The schematic illustration of the draw-bending (so-called *hat-bending*) is shown in **Fig. 5**.

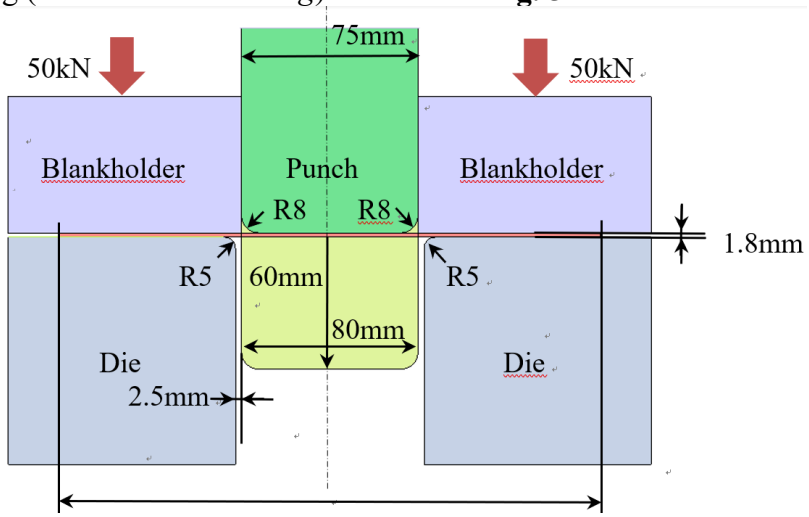

Fig. 5. Schematic illustration of the set-up of hat-bending

Fig.6 illustrates the comparison of measured stress-strain curve and the reproduced stress-strain curve with subloading surface model using the following values of material parameters.
Material constants :

Initial yield stress: $F_0 = 402\text{MPa}$

Elastic moduli: $E = 200{,}000\text{MPa}, \quad \nu = 0.3,$

$$Hardening \begin{cases} isotropic: \ h_1 = 0.75, & h_2 = 15, \\ kinematic: c_k = 250MPa, & \zeta = 1.0, \end{cases}$$

$$Evolution\ of\ normal - yield\ ratio: \bar{u} = 300 \ \ u_c = 5,$$

The good agreement is observed in **Fig. 6** unlike **Fig. 7** that illustrates the comparison of measured one and reproduced one with conventional combined hardening model. Conventional combined hardening model in Marc uses the ratio of isotropic hardening part and kinematic hardening part, 80% for isotropic hardening and 20% for kinematic hardening were used in this case.

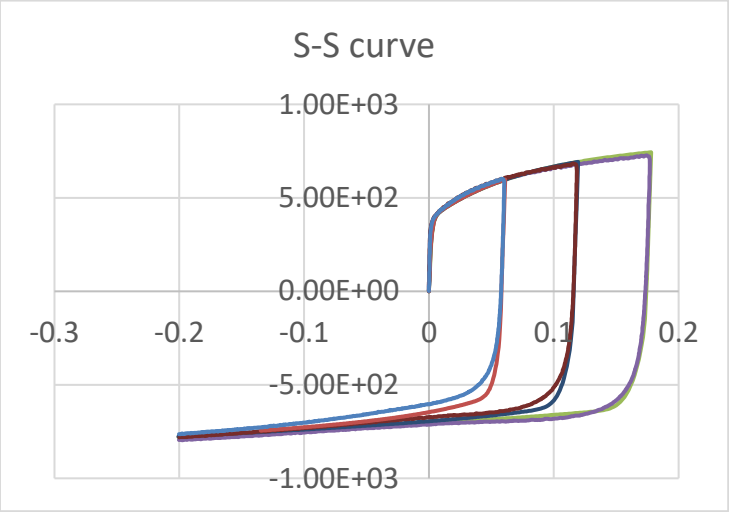

Fig. 6 Measured stress-strain curve and reproduced stress-strain curve with subloading surface model.

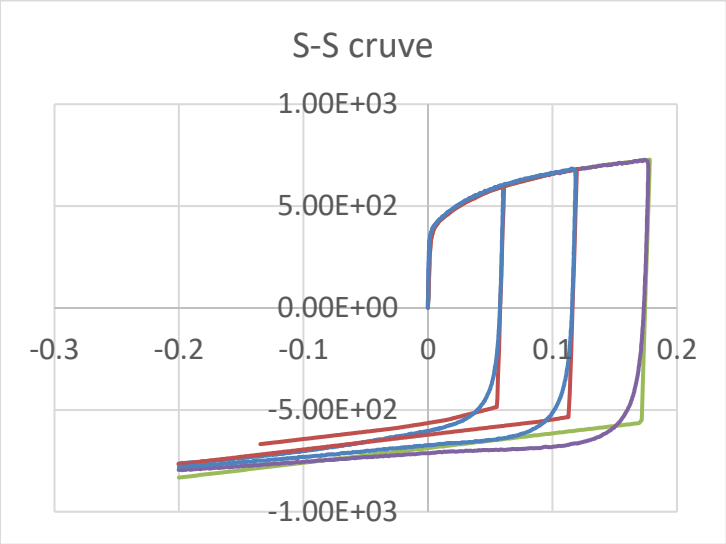

Fig. 7 Measured stress-strain curve and reproduced stress-strain curve with conventional combined hardening model

The calculation results of the shapes of the sheet after the springback are shown in **Fig. 8**, which was analyzed with the subloading surface model in the commercial software Marc (MSC Software, Ltd.). The enough springback is predicted, which is caused by the plastic deformation in the forming process by virtue of the advantage of the subloading surface model describing the plastic strain rate due to the rate of stress inside the yield surface.

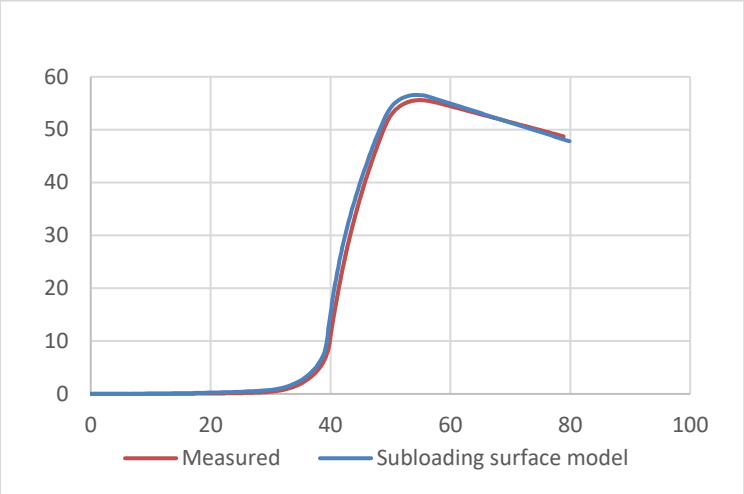

Fig. 8 Springback analysis with subloading surface model

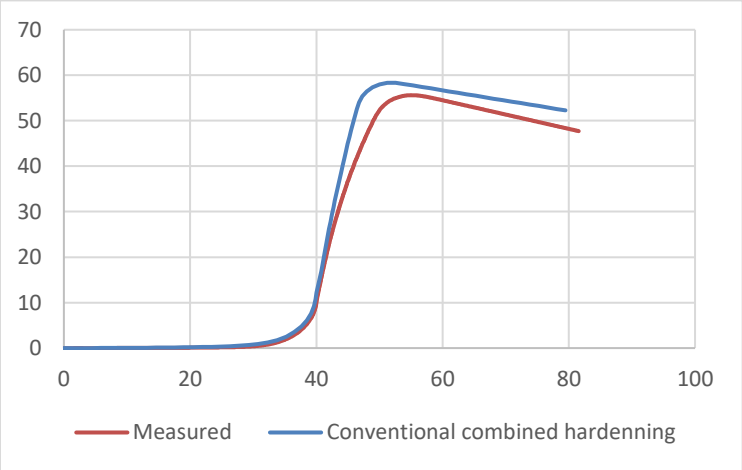

Fig. 9 Springback analysis with conventional combined hardening model

In contrast, the spingback, shown in the **Fig. 9,** is predicted slightly by the conventional elastoplastic model which is realized by using the combined hardening model in Marc. The major reason seems to be luck of accurate reproduction of Bauschinger effect during reverse yielding stage with conventional plasticity model and it is obvious that some part of material is subjected to reverse yielding situation in this type of forming process since initially bended portion, partially tensile yielding state and partially compressive yielding state, will be stretched in the later forming stage, all stretched yielding state. Then, the importance is recognized for the introduction of the rigorous elastoplastic model, i.e. the subloading surface model capable of describing the plastic strain rate in the stress-reducing process appropriately. Hereinafter, it is desirable that the prediction of springback behavior will be executed by the pertinent analysis exploiting the subloading surface model, aiming at the epochal improvement of the prediction of the springback behavior in industries.

5 CONCLUSIONS

The subloading surface elastoplastic constitutive model innovated by Hashiguchi was implemented in Marc general purpose nonlinear finite element commercial software. Implementation of forward Euler based stress integration formulation, that has full functionality to describe plasticity phenomena such as the Masing effect, stagnation and so on, into implicit static software is not easy since typical incremental strain is much larger than the stability limit of Eulerian integrator. In order to preserve unconditionally stable characteristic, we used Strain Subdivide Method as stress integration scheme that subdivide the incremental strain into acceptably small size for stress integrator. During the implementation, several numerical tests were carried out in order to confirm the speed performance and also accuracy using typical industrial problem such as tensile test of dumbbell specimen.

The pringback simulation for sheet metal forming of high strength steel material is performed and the result was compared against the measured result of physical experiment. Throughout this numerical experiment it is confirmed that springback phenomena which has strong dependency on Bauschinger effect can be predicted with subloading elastoplastic constitutive model and the conventional elastoplastic constitutive model has limitation in accuracy for the prediction of springback due to luck of accurate reproduction capability of Bauschinger effect.

REFERENCES

[1] Hashiguchi, K. (1980): Constitutive equations of elastoplastic materials with elastic-plastic transition, *J. Appl. Mech.*, **47**, 266-272.

[2] Hashiguchi, K. (1989): Subloading surface model in unconventional plasticity, *Int. J. Solids Struct.*, **25**, 917-945.

[3] Hashiguchi, K. (2017): *Foundation of Elastoplasticity: Subloading Surface Model*, Springer.

[4] Hashiguchi, K. (2016): Exact formulation of subloading surface model: unified constitutive law for irreversible mechanical phenomena in solids, *Arch. Compt. Meth. Eng.*, **23**, 417-447.

[5] Mroz, Z. (1967): On the description of anisotropic workhardening, *J. Mech. Phys. Solids*, **15**, 163-175.

[6] Dafalias, Y.F. and Popov, E.P. (1975): A model of nonlinearly hardening materials for complex loading, *Acta Mech*., **21**, 173-192.

[7] Chaboche, J.L., Dang-Van, K. and Cordier, G. (1979): Modelization of the strain memory effect on the cyclic hardening of 316 stainless steel, *Trans. 5th Int. Conf. SMiRT*, Berlin, Division L., Paper No. L. 11/3.

[8] MSC Software Corporation (2017): User manual for Hashiguchi model, *Marc and Mentat Release Guide 2017.1, Material Behavior*.

[9] Armstrong, P.J. and Frederick, C.O. (1966): A mathematical representation of the multiaxial Bauschinger effect, *CEGB Report RD/B/N 731* (or in *Materials at High Temperature*, **24**, 1-26 (2007)).

[10] Masing, G. (1926): Eigenspannungen und Verfestigung beim Messing, *Proc. 2nd Int. Congr. Appl. Mech.*, Zurich, pp. 332-335.